



OPEN Sex-specific proximal tubular cell differentiation pathways identified by single-nucleus RNA sequencing

Yueh-An Lu^{1,2,3}, Tanya Smith^{1,2}, Sumukh Deshpande^{1,2}, Chia-Te Liao^{4,5}, Bnar Talabani^{1,2}, Irina Grigorieva^{1,2}, Anna Mason^{1,2}, Robert Andrews¹, Timothy Bowen^{1,2}, Philip R. Taylor^{1,6} & Donald Fraser^{1,2}✉

Postnatal kidney growth is substantial and involves expansion in kidney tubules without growth of new nephrons, which are the functional units of the kidney. Proliferation and differentiation pathways underpinning nephron elongation are not well defined. To address this, we performed sequential characterization of mouse kidney transcriptomics at the single cell level. Single nuclear RNA sequencing (snRNA-seq) was performed on kidney tissue from male and female mice at 1, 2, 4 and 12 weeks of age using the 10x Chromium platform. Unbiased clustering was performed on 68,775 nuclei from 16 animals. 31 discrete cellular clusters were seen, which were identified through comparison of their gene expression profiles to canonical markers of kidney cell populations. High levels of proliferation were evident at early time points in some cell types, especially tubular cells, but not in other cell types, for example podocytes. Proliferation was especially evident in Proximal Tubular Cells (PTCs) which are the most abundant cell type in the adult kidney. Uniquely when compared to other kidney cell types, PTCs demonstrated sex-specific expression profiles at late, but not early, time points. Mapping of PTC differentiation pathways using techniques including trajectory and RNA Velocity analyses delineated increasing PTC specialization and sex-specific phenotype specification. Our single-cell transcriptomics data characterise cellular states observed during kidney growth. We have identified PTC differentiation pathways that lead to sex-specific tubular cell phenotypes. Tubular proliferative responses are of central importance in postnatal kidney growth and have also been linked to kidney recovery versus fibrosis following injury. Our unbiased and comprehensive dataset of tubular cell development can be used to identify candidate pathways for therapeutic targeting.

Keywords Cell biology and structure, Chronic kidney disease, Epithelial, Kidney tubule, MRNA, Proximal tubule, Renal epithelial cell, Renal fibrosis, Renal tubular epithelial cells

The functional unit of the kidney is the nephron, which is dependent for its excretory and homeostatic functions on filtration of the plasma in the glomerulus, followed by selective reabsorption and secretion in tubular segments. The compartmentalized functions of nephron segments are reflected in the highly specialized phenotypes of the different cells contributing to overall nephron composition. Acquisition of these specialized phenotypes underlies nephron formation, a consequence of a series of reciprocal interactions between branching ureteric bud and pretubular aggregate occurring during development¹.

Substantial postnatal growth in kidney size is evident, but underlying cellular processes are comparatively poorly categorized. Kidney growth occurs without increased nephron number in mammals, but nephron length is extended many-fold, and this is associated with extensive proliferation of Proximal Tubular Cells (PTC) and other tubular cell populations. PTC are quantitatively the greatest contributor to cellular composition of the adult kidney, and recent studies employing single nuclear RNA sequencing (snRNA-seq) have uncovered subsets of PTCs with discrete transcriptomic profiles^{2,3}. Profiles matching anatomically distinct PTC segments (S1, S2, S3) and intermediary or overlap profiles are evident. Rare PTC phenotypes, including proliferating and dedifferentiated cells, are seen in injured kidney where they may be key to failed repair processes and to

¹Division of Infection and Immunity, School of Medicine, Cardiff University, Cardiff, UK. ²Wales Kidney Research Unit, School of Medicine, Cardiff University, Heath Park, Cardiff CF14 4XN, UK. ³Division of Nephrology, Kidney Research Center, Linkou Chang Gung Memorial Hospital, Linkou, Taiwan. ⁴Division of Nephrology, Department of Internal Medicine, Taipei Medical University-Shuang Ho Hospital, New Taipei, Taiwan. ⁵Division of Nephrology, Department of Internal Medicine, School of Medicine, College of Medicine, Taipei Medical University, New Taipei, Taiwan. ⁶Dementia Research Institute at Cardiff University, Cardiff, UK. ✉email: fraserdj@cardiff.ac.uk

progression of renal fibrosis^{3,4}. However, such rarer phenotype PTC are also present in normal adult kidney, where their function is less well understood and their low abundance renders them challenging to study.

Important differences exist between the sexes in excretory function, regulation of blood pressure and other homeostatic functions of the kidney⁵, and in risk and outcome of kidney diseases⁶. Sex differences in acid-base homeostasis have been linked to structural and functional differences in male and female proximal tubules⁷, and in a recent study employing a multiomic approach on microdissected mouse PTCs, differences between adult male and female mouse kidney were demonstrated⁸.

Here, we have studied transcriptional profiles at single cell resolution in kidneys from growing mice. We performed snRNA-seq on whole kidney from male and female mice at one, two, four and twelve weeks of age. Profound proliferation and increased abundance of differentiating cellular phenotypes has enabled study of PTC differentiation pathways. We delineate undifferentiated phenotypes that appear early in the post-proliferation trajectory of PTC differentiation and are common between males and females, and later mature phenotypes exhibiting significant sexual dimorphism associated with alterations in the cellular metabolic profile.

Methods

C57BL/6 mice

Experimental work was carried out using male and female C57BL/6 mice aged 1, 2, 4, and 12 weeks old from Charles River Laboratories. The 1, 2 and 4 week old mice were bred in-house by mating the C57BL/6 adult mice. Mice were housed with free access to chow and tap water on a 12 h day/night cycle in a specific pathogen free environment. No *a priori* criteria were established for exclusion of animals, and none were excluded from the experiments or dataset. After mice were euthanized using Isoflurane, chilled PBS (1x) perfusion via left ventricle was performed before kidney harvest. Body weight, kidney weight and kidney length were recorded. Kidneys from two male and two female healthy mice at all ages were processed for snRNA-seq. Hematoxylin and Eosin staining was performed on formalin-fixed, paraffin-embedded kidney sections. Experiments were performed in accordance with ARRIVE guidelines (<https://arriveguidelines.org>) and in line with institutional and UK Home Office guidelines under the authority of an appropriate project license. The specific experimental protocol was not published prior to the study.

Tissue collection and isolation of nuclei

For nuclear isolation for the snRNA-seq experiments, the 1 and 2 week old mouse kidneys were processed using a whole kidney, the 4 week old mouse kidneys were processed using half of a kidney and the 12 week old organs were processed using a quarter of a kidney from each mouse. The kidneys were minced into < 2 mm pieces and transferred to a Dounce tissue grinder containing 2 ml of lysis buffer (Nuclei EZ Lysis buffer, Sigma NUC101) supplemented with protease inhibitor (Sigma 5892970001) and RNase inhibitors (Promega N2615 and Life Technologies AM2696). Kidneys were homogenized and transferred into 50 ml tubes containing 2 ml of lysis buffer and incubated for 7 min on ice. The lysed cells were filtered through a 40- μ m cell strainer and centrifuged at 500g for 5 min at 4°C. The supernatants were removed, the pellets were resuspended in 4 ml of lysis buffer, incubated for another 7 min on ice, then centrifuged again at 500g for 5 min at 4°C. The supernatants were removed, the pellets were resuspended in 4 ml of wash & resuspension buffer (1xPBS, 1.0% BSA, and RNase Inhibitor (Sigma 3335399001)) and filtered through a 20- μ m cell strainer. Samples were then processed immediately using the 10x Genomics single-cell library preparation protocol.

Library preparation and RNA sequencing

Library preparation was performed using Chromium Single Cell 3' Reagent Kits v3.1 (10x Genomics). cDNA quality was evaluated by fragment analysis (5200 Fragment Analyzer System, Agilent). RNA sequencing was carried out using the Illumina NovaSeq System.

Data processing and core analysis of snRNA-seq dataset

The sequencing data were processed using the zUMIs pipeline (version 2.3.0)⁹. The pipeline was used to first discard reads with low-quality barcodes and UMIs, and then to map reads to the mouse reference assembly (Mus_musculus.GRCm38.95). zUMIs outputted the data matrix as an rds file for downstream analysis in R. Genome mapping and gene counting were performed on the Cardiff University high performance computing cluster (Hawk). The barcode-gene matrix generated by zUMIs was analyzed using the R package, Seurat (version 4.3.0)^{10,11}.

In Seurat, cells for individual samples were retained if they contained ≥ 200 genes and genes identified in ≥ 3 nuclei. Data from all 16 mouse kidneys were merged. Cells were filtered again to remove nuclei expressing ≤ 600 genes or ≥ 7500 genes, or with mitochondrial gene expression $\geq 7.5\%$. Quality Control plots are shown in Supp Fig. 1A & B. The related data information is shown in Supplementary Data 1. The feature counts were normalized with scale factor = 10,000. The top 2,000 variable genes were identified and scaled, and the principal component analysis (PCA) result of the scaled data was obtained. The data was then processed using Harmony (version 0.1.1) for batch effect correction^{12,13}. *FindNeighbors* and *FindClusters* functions were applied based on previously corrected principal components (PCs) to identify clusters of nuclei. The number of PCs included in the downstream analysis was determined by identifying the knee point of the elbowplot generated after running *the JackStraw* procedure. To visualise the dataset in low-dimensional space, the *RunTSNE* function was used to generate a t-Distributed Stochastic Neighbor Embedding (t-SNE) plot, and the *RunUMAP* function was used to generate a Uniform Manifold Approximation and Projection (UMAP) plot. An R package, DoubletFinder (version 2.0.2) was used to predict and exclude dubious doublets in the dataset¹⁴. After doublet removal, the merged dataset was again normalized, scaled, processed with PCA and Harmony. The PCA before and after

Harmony are shown in Supp Fig. 1. Final clustering results were visualized using UMAP. *DotPlot* function was used to show the expression level and percentage of genes expressed among different clusters.

FindMarkers command (Wilcox method as the default) to identify canonical cell type marker genes of each cluster. Significance was defined using the default recommended parameters, which are a gene with an adjusted p-value < 0.05, $a \geq 0.25$ average log fold difference between the two groups of cells, and presence detected in at least 10% of cells in either of the two populations. P-value adjustment was performed using Bonferroni correction based on the total number of genes in the dataset.

The cell cycle analysis used *CellCycleScoring* to identify cells in the G2/M and S status. Cells with G2M.Score > 0.15 and G2M.Score > S.Score were assigned as G2M status. Cells with S.Score > 0.15 and S.Score > G2M.Score were assigned as S status. Cell with G2M.Score < 0.15 and S.Score < 0.15 were assigned as G1/G0 phase.

Proximal tubular cell subclustering analysis

The PTC clusters were subset for further analysis. PTCs of 1, 2, 4 and 12 week old mouse kidneys were integrated using Seurat. The integrated dataset was then scaled and processed with PCA, *FindNeighbors* and *FindClusters*. A total of 30,396 PTCs were re-clustered and analyzed. PTCs were discriminated into 26 clusters (Supp Fig. 2A). Results of the re-clustering were compatible with the primary results of cell-type identification (Supp Fig. 2B). A cluster containing 242 cells that expressed both PTC and endothelial marker genes (*Flt* and *Emcn*) and had higher genes per cell was removed as highly suspicious of residual doublets (Supp Fig. 2C-D). Marker genes of the new PTC clusters were identified using differential gene expression (DGE) analysis. For DGE analysis, we used the *FindMarker* command. Significance was defined as a gene with an adjusted p value < 0.05, $a \geq 0.25$ average log2-fold difference between the two groups of cells, and whose presence was detected in at least 10% of cells in either of the two populations. P-value adjustment was performed using Bonferroni correction based on the total number of genes in the dataset. The remaining clusters were combined into 15 defined clusters.

Velocity and pseudotime analysis

The RNA velocity of PTCs was calculated by *velocyto.py* and *velocyto.R* (version 0.6) using the spliced and unspliced RNA counts provided by 10X cellranger package¹⁵. The R package Monocle3 (Monocle 3 version 1.3.0) was used for trajectory and pseudotime analysis¹⁶. The trajectory analysis of the re-clustered PTCs was performed using the *learn_graph* function. Pseudotime analysis was performed based on the RNA velocity result.

KEGG pathway analysis

We conducted gene set enrichment analysis (GSEA) to understand pathways characteristic of the PTC clusters using the R package, WebGestaltR (version 0.4.3)¹⁶. We evaluated the pathway enrichment in the KEGG functional databases using the recommended False Discovery Rate (FDR) cutoff of 0.25 (<https://www.gsea-msigdb.org/gsea/index.jsp>).

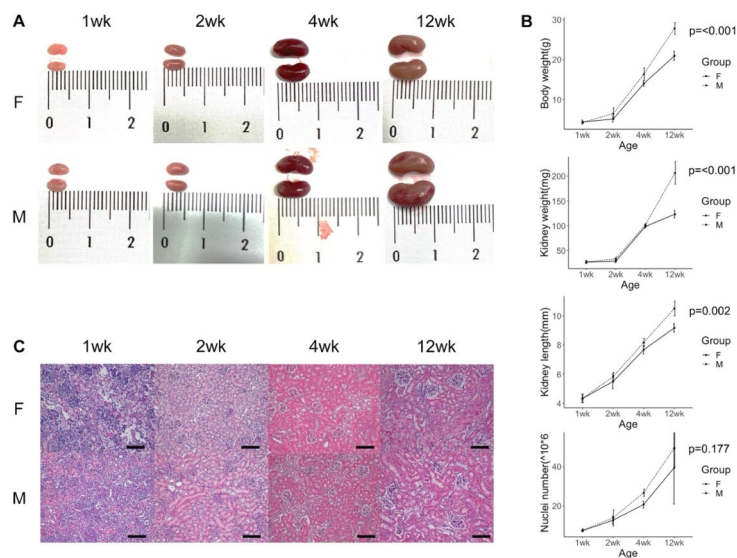


Fig. 1. Appearances of female and male mouse kidneys at 1, 2, 4 and 12 weeks of age. (A) Kidneys freshly harvested from female (F) and male (M) mice at different ages. Ruler scale is shown in centimeters. The length and size of kidneys increased with age. (B) Line charts of body weight, kidney weight, kidney length and extracted number of nuclei from female and male mouse kidneys at different ages ($n = 3$ of each group at each time point). Data is shown as mean \pm standard deviation. Adult male mice had higher body weight, higher kidney weight and kidney length than adult female mice (Bonferroni Post-hoc-Tests). (C) H&E stain of female and male kidneys at different ages (scale = 100 μ m). Tubular expansion was observed during growth.

Results

Kidney growth was evaluated in male and female mice. Macroscopic appearances of whole kidneys are shown (Fig. 1A). Increases in body weight, kidney weight, kidney length and number of nuclei extracted from whole kidney were seen from 1 to 12 weeks in age and, by 12 weeks, males exhibited greater values for body weight, kidney weight and kidney length than females (Fig. 1B). Histological appearances of female and male kidneys at each time point are depicted in Fig. 1C.

SnRNA-seq was performed on kidney tissue from male and female mice at 1, 2, 4 and 12 weeks of age. Unbiased clustering was performed on 68,775 nuclei, revealing 31 separate clusters (Fig. 2A). Cluster identification was performed using canonical marker genes (Fig. 2B). Kidneys of different ages and sexes varied in the proportional contribution to cellular number of each cluster (Fig. 2A, Supp Figs. 3, 4 and 5). Cell cycle status identified cells in G2/M and S phase versus those in G1 (Fig. 2C). While tubular nephron segments exhibited abundant proliferation, proliferation of other cells was less evident. Alterations in overall cellular composition over time were evident, with some clusters contributing a greater proportion of total cell number at early time points, including proliferating cells of various lineages (Fig. 2E, Supp Fig. 6) as well as podocytes, mesangial cells, endothelial cells, juxtaglomerular cells and fibroblasts (Fig. 2F, Supp Fig. 6). In contrast, the proportion of total cell number that were tubular cells of various types increased throughout kidney growth (Fig. 2G, Supp Fig. 6).

The data demonstrated substantial numbers of proliferating PTCs at early time points, and increasingly dominant contribution to overall kidney cell number of PTCs at later time points (Fig. 2E–G). Comparison of overall data further demonstrated differences between male and female animals in PTC clusters but not in clusters of other phenotypes (Supp Fig. 4). Recent work from the Knepper laboratory has found important sexual dimorphism in microdissected proximal tubular segments using a multiomic approach⁸. Therefore, we next reclustered and analysed PTC. Before commencing this analysis, we sought to confirm the presence of proliferating cells across PTC segments. Ki67 was used as a marker of proliferating cells, while Slc5a2, Slc13a3 and Slc5a10 were used to identify PT segments S1, S2, and S3, respectively. Ki67-positive cells were found to be localized to S1, S2 and S3 PTC segments (Fig. 3A–C).

X-inactive specific transcript (Xist) is a long noncoding RNA that is expressed from the inactive X Chromosome in female cells, and functions as a central component of the X chromosome inactivation machinery that transcriptionally silences one of the two X chromosomes present in female cells¹⁷. Maternal microchimerism leads to the presence of a small proportion of maternal cells in the fetus, which persist in adult tissues and may have important developmental and functional consequences¹⁸. In this dataset, Xist was detected in 91.1% of cells from female animals and 0.3% of cells from male animals. Cells expressing Xist, whether from female mice or from male mice and of presumed maternal origin, demonstrated unequal distribution in the PTC clusters, but not in other nephron segments (Fig. 2D).

Next, PTC reclustering analysis was performed (Fig. 4A, Supp Figs. 2, 7 and 8). 15 PTC clusters were identified, of which 11 were comprised of Xist-positive and -negative cells, while 4 exclusively contained Xist-negative cells (Fig. 4A and C). Cluster annotation was performed using expression of canonical anchor genes (Fig. 4B, Supp Figs. 9 and 10). The transcriptional profile of the clusters identified cells of S1, S2, and S3 segment phenotype, together with “intermediate” phenotypes exhibiting S1/2 and S2/3 markers. Three separate proliferating clusters were observed, labelled “ProlifPT_1, 2, and 3”. Two undifferentiated clusters were seen, the first labelled “PT_Immature” and the second exhibiting overlap with a cluster that we have previously identified as comprising dedifferentiated PTC together with parietal epithelial cells³, here labelled “PTdediff_PEC”. Comparison of gene expression in male and female PTCs demonstrated comparatively few differentially expressed genes at 1 week and 2 week time points, but at 4 week and 12 week time points, increasing sexual dimorphism was evident (Fig. 4D).

Velocity analysis, which infers rate and direction of change in transcriptomic profile from systematic comparison of unspliced to spliced mRNA ratios¹⁵, was performed on the reclustered PTCs. Undifferentiated and proliferating clusters exhibited high levels of change in transcriptional profile, while the transcriptional

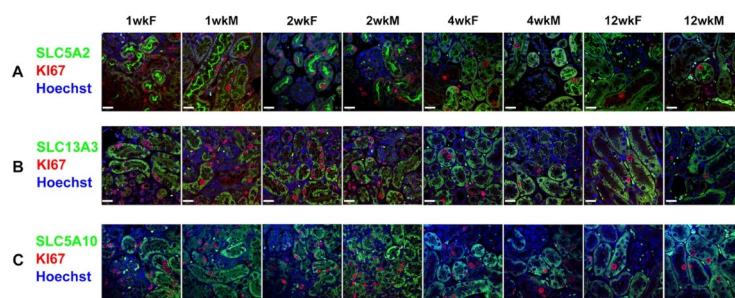


Fig. 3. Validation of the snRNA-seq result using immunofluorescence stain of the proliferative cells in S1, S2 and S3 segments of the proximal tubule. Immunofluorescence stain shows the colocalization of the proliferative marker Ki67 and the PTC markers for S1 segment, SLC5A2 (A); S2 segment, SLC13A3 (B) and S3 segment, SLC5A10 (C) (scale = 20 μ m). Proliferating cells were identified in S1, S2 and S3 segments at 1, 2, 4, and 12 weeks-old male and female mice. The image is representative of 2 mice in each group. High proliferation was noted postnatally and reduced as the tissue matures in all three PT segments under microscope.

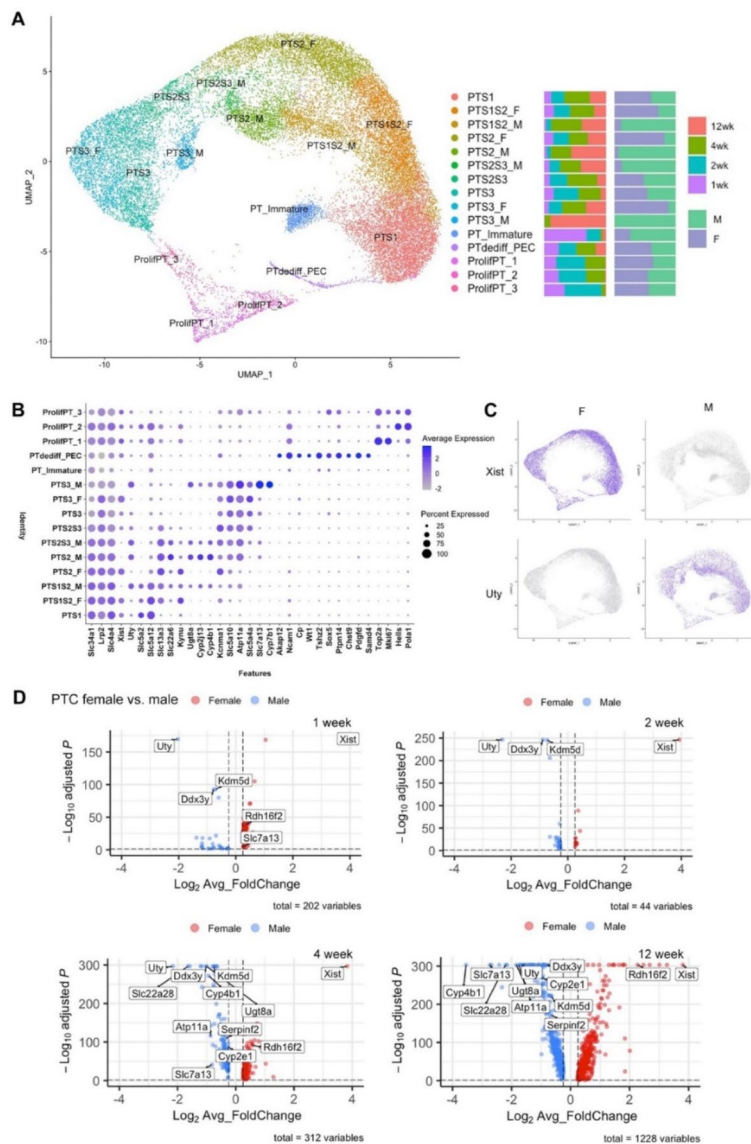


Fig. 4. Analysis of PTCs of female and male mouse kidneys at 1, 2, 4 and 12 weeks of age. **(A)** Result of PTC re-clustering is shown using UMAP plot. **(B)** Dotplot shows the expression levels and the percentage of gene expression of the canonical genes in each of the PTC clusters. **(C)** Feature plot of the expression of *Xist* and *Uty* genes, which are specific for female and male cells, respectively. **(D)** Volcano plots show the results of differential expression gene (DEG) analysis of female and male PTCs at different ages. Twelve of the top 30 most differentially expressed genes are annotated, based on their comparatively high expression. These include *Cyp2e1*, *Cyp4b1*, *Ddx3y*, *Kdm5d*, *Atp11a*, *Rdh16f2*, *Serpinf2*, *Slc22a28*, *Slc7a13*, *Ugt8a*, *Uty*, and *Xist*.

profiles of mature PTC phenotypes appeared more stable (Fig. 5A). The velocity analysis suggested two arrow flows, one from ProlifPT to PTS3 and the other from ProlifPT to PTS1 (Fig. 5A). Pseudotime analysis was used to determine PTC differentiation pathways. Pseudotime origin was specified as proliferating PT (Fig. 5B). Ordering of cells along a latent (pseudotime) axis demonstrated a trajectory from proliferating through undifferentiated to mature phenotypes, the latter ordered anatomically from S1 to S3, indicating that the PT in S3 clusters were most transcriptionally different from proliferating PT (Fig. 5B). *Xist*-specific clusters also segregated late in the trajectory. Expression along the pseudotime demonstrated that following transient expression of proliferation-associated genes including *Mki67*, cells exhibited undifferentiated profiles followed by expression of markers of a fully differentiated phenotype (Fig. 5C). Repeating the pseudotime with alternate origins gave similar results (Suppl Figs. 11, 12). The final, differentiated phenotypes were suggested by RNA Velocity analysis to be comparatively transcriptionally stable (Fig. 5A).

We next evaluated the 12 genes found to be abundantly expressed amongst those differentially expressed between male and female PTCs. 4 genes (*Xist*, *UTY*, *Kdm5d* and *Ddx3y*) were highly differentially expressed by male or female cells throughout, consistent with their localization on sex chromosomes and known roles in female/male cell specification^{8,19}. In comparison, genes originating on autosomes (*Rdh16f2*, *Serpinf2*, *Slc22a28*,

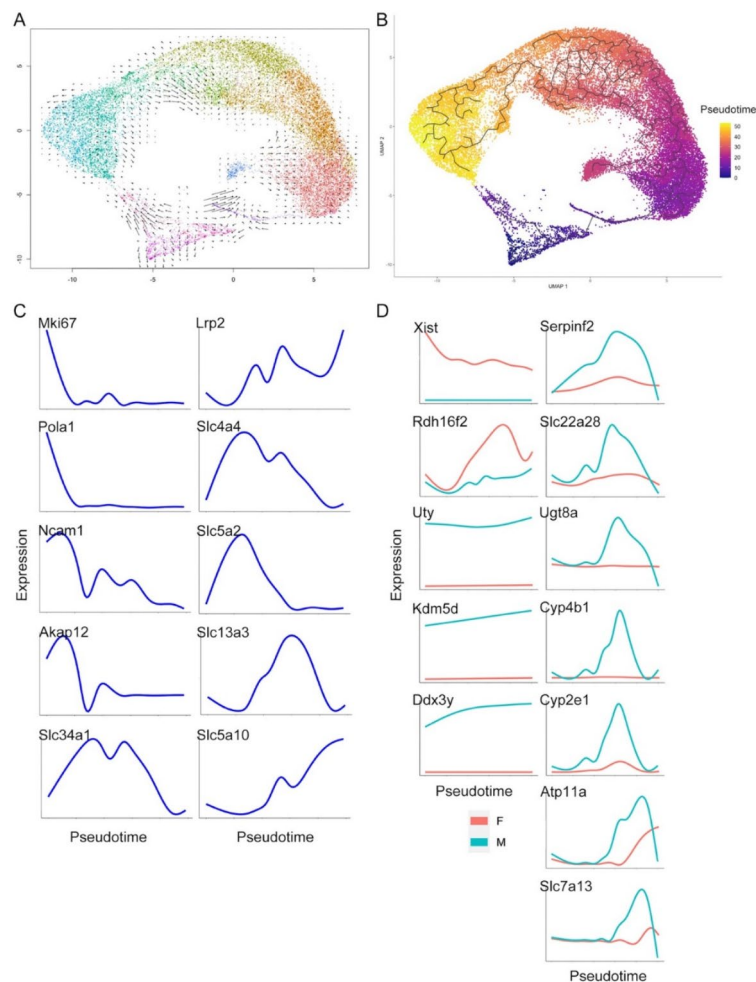


Fig. 5. Velocity and pseudotime analysis. **(A)** Velocity analysis shows that PTCs differentiation starts from proliferative PTCs and goes toward S1 and S3. **(B)** Result of pseudotime analysis. **(C)** Gene expression along pseudotime of marker genes of the PTC clusters. **(D)** Expression of genes selected from the DEG analysis, plotted along pseudotime in female and male mouse kidneys. *Xist*, *Uty*, *Ddx3y* and *Kdm5d* were persistently expressed throughout PTC differentiation whereas other genes demonstrate restricted expression patterns.

Ugt8a, *Cyp4b1*, *Cyp2e1*, *Atp11a*, *Slc7a13*) were differentially expressed later in pseudotime (Fig. 5D). Similar results were obtained with the alternate proliferating and undifferentiated pseudotime origins (Suppl Fig. 12).

We next evaluated the high-level functions evident in the PTC clusters by KEGG analysis²⁰. Comparing 1 week and 12 week cells, 1 week cells exhibited enrichment for metabolic pathways, while 12 week cells were enriched in pathways including cell cycle regulation, adhesion, ECM interaction, and mineral absorption (Fig. 6A). Male and female PTCs were similar at early time points but exhibited distinct transcriptional profiles at 12 weeks. KEGG analysis comparing 12-week male and female cells demonstrated that pathways comparatively upregulated in male cells included oxidative phosphorylation, arachidonic acid metabolism, metabolic pathways, and ribosome synthesis (Fig. 6B). These data identify important differences in transcriptional profile, and in pathway activity between mature male and female PTCs.

Discussion

Here we have performed snRNA-seq on postnatal mouse kidney at time points from one to twelve weeks. In this time period, nephron number is fixed but kidney size, and individual nephron length, increase substantially. The data delineate the discrete cellular transcriptomic profiles present in the mouse kidney during postnatal growth. They further uncover important differences between mature male and female PTCs.

PTC and other differentiated kidney cell phenotypes arise during nephron formation. In the mammalian kidney, acquisition of the specialized phenotypes required for different nephron regions requires the reciprocal interactions of branching ureteric bud and pretubular aggregate²¹. Epithelialization of the pretubular aggregate forms the renal vesicle, from which the nephron then forms²². In humans all nephrons have been formed by 34–37 weeks' gestation²³. In mice, nephron formation has been observed up to postnatal day 4²¹.

Imaging studies and single cell RNA sequencing have shown that during nephrogenesis, progenitor cells are gradually recruited, and trajectory analysis demonstrates transcriptomic divergence as distinct regions

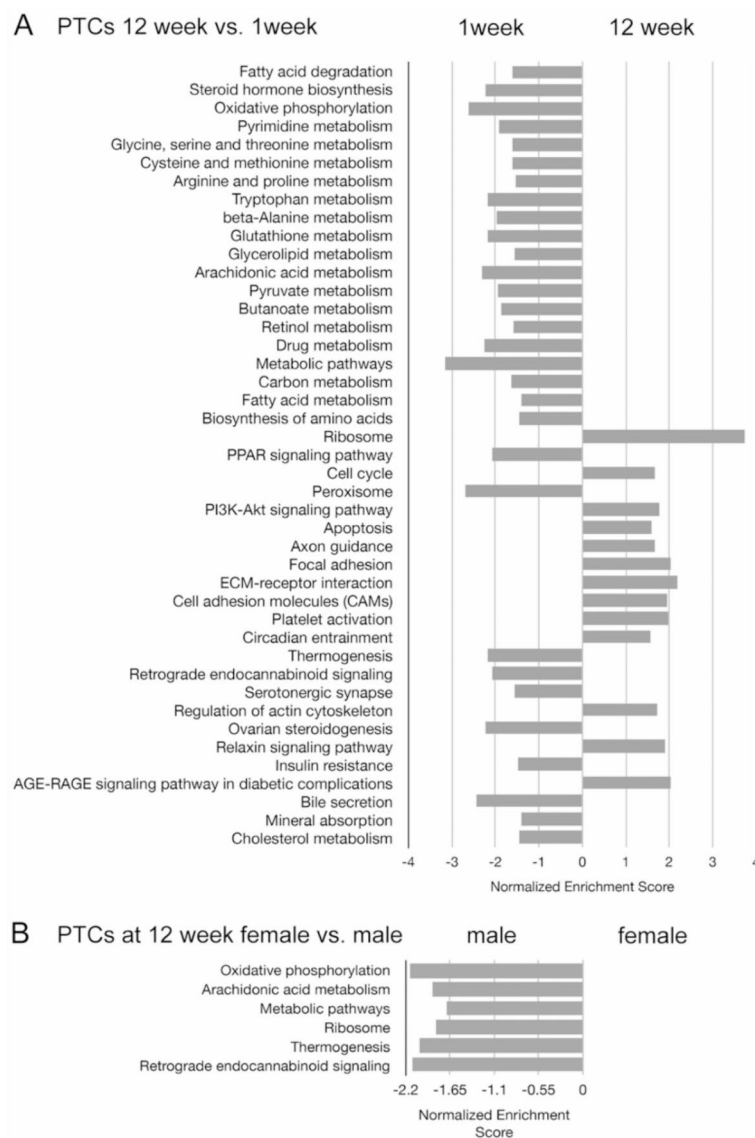


Fig. 6. Pathway analysis of PTCs based on the KEGG database of (A) 12 week vs. 1 week and (B) female vs. male PTCs at 12 weeks old. Results show enriched metabolic pathway expression at 1 week old and enriched cell cycle and cellular community pathway expression at 12 weeks old. Pathways with a false discovery rate < 0.25 were listed. Male cells exhibited enriched energy metabolism and metabolic pathway expression when compared to female cells at 12 weeks old. Pathway analysis utilized the Kyoto Encyclopedia of Genes and Genomes (Kanehisa M et al. *Nucleic Acids Res* 2023; DOI <https://doi.org/10.1093/nar/gkac963>).

of the nephron form²⁴. Our data demonstrate important differences in postnatal cellular composition of the growing kidney, and suggest that postnatally, cellular differentiation continues at a different rate for different nephron regions and their respective cell populations. In support of this, previous studies have shown that while podocytes exhibit early commitment and terminal differentiation, tubular cells exhibit later and more complex differentiation pathways²⁵. SnRNA-seq studies in adult mouse kidney have demonstrated unique profiles for tubular segments, together with presence of a quantitatively small proportion of cells exhibiting proliferative and less fully differentiated PTC phenotypes^{2,3,26}. These minority phenotypes are seen in increased number following kidney injury, where additional pathology-associated phenotypes may be seen^{3,4,27}. The rare nature of such cells in mature kidney outside of injury makes their profiling and determination of phenotype a challenge. The sequential profiling of growing kidney presented here, where proliferating and not yet fully differentiated phenotypes comprise a greater proportion of cell number, has uncovered the inter-relationships and development pathways of PTCs during kidney growth. These data map gene expression along a development pathway that proceeds from proliferation through intermediary phenotypes to cells with a mature, and anatomically restricted, expression profile.

Pathway analysis of PTCs based on the KEGG database identified comparatively high expression of metabolic pathways at early postnatal timepoints, whereas at later time points, PTCs demonstrated enrichment of

pathways including those related to cellular adhesion and circadian entrainment. The data further demonstrate differences between cellular transcriptomic profiles in male and female kidney, that appear largely restricted to PTCs. Comparison of male and female PTC revealed relatively few differentially expressed genes at 1 and 2 week timepoints, while at 4 week and 12 week time points, increasing numbers of differentially expressed genes were found. Evaluation of sequential time points demonstrated sequential recruitment of genes that then remained differentially expressed in male and female PTCs at later time points. Pathway analysis highlighted enriched energy metabolism and metabolic pathway expression in male PTC, and these findings are in broad agreement with previous work, in particular that of Ransick et al.¹⁹ showing distinct PT expression patterns and highlighting metabolic gene expression differences between the sexes.

Quantitative immunoblotting in adult rat kidney has previously demonstrated sex differences in renal transporters and electrolyte homeostasis²⁸ and recent data from protocol transplant donor kidney biopsies identified increased metabolic activity of male PTC, supporting that this may also be found in human kidney²⁹. In the current dataset, the genes identified as differentially expressed from 1 week notably included several genes located on sex chromosomes and with core roles in processes including X chromosome inactivation in female cells. 8 other genes, located on autosomes, were identified as abundantly expressed in kidney and exhibiting sexual dimorphism in PTCs at later time points (*Rdh16f2* in female PTCs, and *Serpinf2*, *Slc22a28*, *Ugt8a*, *Cyp4b1*, *Cyp2e1*, *Atp11a*, *Slc7a13* in male PTCs). These differences in PTC transcriptomic profile may underlie known differences in female versus male kidney responses to injury. For example, *Rdh16f2* expression, enriched in female PTCs at a late stage in the current dataset, is downregulated in male mice compared to female mice following ischemic injury³⁰ and is linked to protective preconditioning in this context³¹.

Maternal microchimerism may represent an additional source of complexity in the male versus female patterning of the proximal tubular component of the nephron. Maternal microchimerism is the presence of a small proportion of cells of maternal origin in the progeny and is a result of vertical transmission of maternal cells to the fetus during mammalian pregnancy. The data presented here support the presence of maternal microchimerism in mouse kidney and suggest that in male animals, such maternal-origin cells retain transcriptionally female profiles in the proximal tubule. While the number of cells is quantitatively small, data supports the importance of maternal microchimerism in patterning other organs and suggests that this warrants further study in kidney. For example, maternal microchimerism has recently been found to promote brain development and homeostasis in mice¹⁸.

In summary, these data provide an atlas of transcriptomic data in the growing postnatal mouse kidney. They demonstrate that while postnatal cell proliferation is limited or absent for some cellular subtypes during mouse kidney growth, high levels of proliferation are present for others, including PTC. The results further highlight important sex differences in PTC differentiation pathways and differentiated PTC phenotype, which may have important implications for observed sex differences in outcome following acute kidney injury, experimentally and clinically.

Data availability

Data is uploaded to a publicly available repository and freely available following publication. (<https://www.ebi.ac.uk/biostudies/arrayexpress/studies/E-MTAB-13284>).

Received: 5 February 2024; Accepted: 13 September 2024

Published online: 14 October 2024

References

- McMahon, A. P. Chapter three - development of the mammalian kidney. In: *Current Topics in Developmental Biology*. edited by Wassarman PM, Academic Press, pp 31–64 (2016).
- Wu, H., Kirita, Y., Donnelly, E. L. & Humphreys, B. D. Advantages of single-nucleus over single-cell RNA sequencing of adult kidney: Rare cell types and Novel Cell States revealed in fibrosis. *J. Am. Soc. Nephrol. JASN*. **30**, 23–32. <https://doi.org/10.1681/ASN.2018090912> (2019).
- Lu, Y. A. et al. Single-nucleus RNA sequencing identifies new classes of proximal tubular epithelial cells in kidney fibrosis. *J. Am. Soc. Nephrol. JASN*. **32**, 2501–2516. <https://doi.org/10.1681/ASN.2020081143> (2021).
- Kirita, Y., Wu, H., Uchimura, K., Wilson, P. C. & Humphreys, B. D. Cell profiling of mouse acute kidney injury reveals conserved cellular responses to injury. *Proc. Natl. Acad. Sci. U S A*. **117**, 15874–15883. <https://doi.org/10.1073/pnas.2005477117> (2020).
- Layton, A. T. & Sullivan, J. C. Recent advances in sex differences in kidney function. *Am. J. Physiol. Ren. Physiol.* **316**: F328–F331, <https://doi.org/10.1152/ajprenal.00584.2018> (2019).
- Kovesdy, C. P. Epidemiology of chronic kidney disease: An update 2022. *Kidney Int. Suppl. (2011)* **12**, 7–11. <https://doi.org/10.1016/j.kisu.2021.11.003> (2022).
- Harris, A. N. & Weiner, I. D. Sex differences in renal ammonia metabolism. *Am. J. Physiol. Ren. Physiol.* **320**: F55–F60, <https://doi.org/10.1152/ajprenal.00531.2020> (2021).
- Chen, L., Chou, C. L., Yang, C. R. & Knepper, M. A. Multiomics analyses reveal sex differences in mouse renal proximal subsegments. *J. Am. Soc. Nephrol. JASN*. **34**, 829–845. <https://doi.org/10.1681/ASN.0000000000000089> (2023).
- Parekh, S., Ziegenhain, C., Vieth, B., Enard, W. & Hellmann, I. zUMIs - A fast and flexible pipeline to process RNA sequencing data with UMIs. *Gigascience*. **7** <https://doi.org/10.1093/gigascience/giy059> (2018).
- Stuart, T. et al. Comprehensive integration of single-cell data. *Cell* **177**, 1888–1902. <https://doi.org/10.1016/j.cell.2019.05.031> (2019) (e1821, 2019).
- Butler, A., Hoffman, P., Smibert, P., Papalexi, E. & Satija, R. Integrating single-cell transcriptomic data across different conditions, technologies, and species. *Nat. Biotechnol.* **36**, 411–420. <https://doi.org/10.1038/nbt.4096> (2018).
- Tran, H. T. N. et al. A benchmark of batch-effect correction methods for single-cell RNA sequencing data. *Genome Biol.* **21**(12). <https://doi.org/10.1186/s13059-019-1850-9> (2020).
- Korsunsky, I. et al. Fast, sensitive and accurate integration of single-cell data with harmony. *Nat. Methods* **16**, 1289–1296. <https://doi.org/10.1038/s41592-019-0619-0> (2019).
- McGinnis, C. S., Murrow, L. M. & Gartner, Z. J. DoubletFinder: Doublet detection in single-cell RNA sequencing data using artificial nearest neighbors. *Cell. Syst.* **8**, 329–337. <https://doi.org/10.1016/j.cels.2019.03.003> (2019) (e324).

15. La Manno, G. et al. RNA velocity of single cells. *Nature*. **560**, 494–498. <https://doi.org/10.1038/s41586-018-0414-6> (2018).
16. Cao, J. et al. The single-cell transcriptional landscape of mammalian organogenesis. *Nature*. **566**, 496–502. <https://doi.org/10.1038/s41586-019-0969-x> (2019).
17. Penny, G. D., Kay, G. F., Sheardown, S. A., Rastan, S. & Brockdorff, N. Requirement for Xist in X chromosome inactivation. *Nature*. **379**, 131–137. <https://doi.org/10.1038/379131a0> (1996).
18. Schepanski, S. et al. Pregnancy-induced maternal microchimerism shapes neurodevelopment and behavior in mice. *Nat. Commun.* **13**, 4571. <https://doi.org/10.1038/s41467-022-32230-2> (2022).
19. Ransick, A. et al. Single-cell profiling reveals sex, lineage, and regional diversity in the mouse kidney. *Dev. Cell*. **51**(e397), 399–413. <https://doi.org/10.1016/j.devcel.2019.10.005> (2019).
20. Kanehisa, M., Furumichi, M., Sato, Y., Kawashima, M. & Ishiguro-Watanabe, M. KEGG for taxonomy-based analysis of pathways and genomes. *Nucleic Acids Res.* **6**, 51: D587–D592. <https://doi.org/10.1093/nar/gkac96> (2023).
21. Short, K. M. et al. Global quantification of tissue dynamics in the developing mouse kidney. *Dev. Cell*. **29**, 188–202. <https://doi.org/10.1016/j.devcel.2014.02.017> (2014).
22. McMahon, A. P. Development of the mammalian kidney. *Curr. Top. Dev. Biol.* **117**, 31–64. <https://doi.org/10.1016/b.sctdb.2015.10.010> (2016).
23. Lindstrom, N. O. et al. Conserved and divergent features of human and mouse kidney organogenesis. *J. Am. Soc. Nephrol.* **29**, 785–805. <https://doi.org/10.1681/ASN.2017080887> (2018).
24. Lindstrom, N. O. et al. Progressive recruitment of mesenchymal progenitors reveals a time-dependent process of cell fate acquisition in mouse and human nephrogenesis. *Dev Cell*, 45: 651–660 e654, (2018). <https://doi.org/10.1016/j.devcel.2018.05.010>
25. Miao, Z. et al. Single cell regulatory landscape of the mouse kidney highlights cellular differentiation programs and disease targets. *Nat. Commun.* **12**, 2277. <https://doi.org/10.1038/s41467-021-22266-1> (2021).
26. Park, J. et al. Single-cell transcriptomics of the mouse kidney reveals potential cellular targets of kidney disease. *Science*. **360**, 758–763. <https://doi.org/10.1126/science.aar2131> (2018).
27. Balzer, M. S. et al. Single-cell analysis highlights differences in druggable pathways underlying adaptive or fibrotic kidney regeneration. *Nat. Commun.* **13**, 4018. <https://doi.org/10.1038/s41467-022-31772-9> (2022).
28. Veiras, L. C. et al. Sexual dimorphic pattern of renal transporters and electrolyte homeostasis. *J. Am. Soc. Nephrol.* **28**, 3504–3517. <https://doi.org/10.1681/ASN.2017030295> (2017).
29. McEvoy, C. M. et al. Single-cell profiling of healthy human kidney reveals features of sex-based transcriptional programs and tissue-specific immunity. *Nat. Commun.* **13**, 7634. <https://doi.org/10.1038/s41467-022-35297-z> (2022).
30. Vinas, J. L. et al. Sex diversity in proximal tubule and endothelial gene expression in mice with ischemic acute kidney injury. *Clin. Sci. (Lond)*. **134**, 1887–1909. <https://doi.org/10.1042/CS20200168> (2020).
31. Johnsen, M. et al. The integrated RNA landscape of renal preconditioning against Ischemia-reperfusion injury. *J. Am. Soc. Nephrol.* **31**, 716–730. <https://doi.org/10.1681/ASN.2019050534> (2020).

Acknowledgements

We would like to thank the staff of our animal facility for the care of the animals used in this study. P.R.T is funded by the Wellcome Trust Investigator Award (107964/Z/15/Z) and the UK Dementia Research Institute. Y.L is funded by Chang Gung Memorial Research Program (CMRPG3N0361).

Author contributions

YAL, DF, PT, TB conceived and designed the experiments YAL, IG, TS performed the experimental work YAL, SD, AM, RA, DF analysed data YAL, DF wrote the initial draft All authors reviewed and revised the manuscript.

Declarations

Competing interests

The authors declare no competing interests.

Additional information

Supplementary Information The online version contains supplementary material available at <https://doi.org/10.1038/s41598-024-73102-7>.

Correspondence and requests for materials should be addressed to D.F.

Reprints and permissions information is available at www.nature.com/reprints.

Publisher's note Springer Nature remains neutral with regard to jurisdictional claims in published maps and institutional affiliations.

Open Access This article is licensed under a Creative Commons Attribution 4.0 International License, which permits use, sharing, adaptation, distribution and reproduction in any medium or format, as long as you give appropriate credit to the original author(s) and the source, provide a link to the Creative Commons licence, and indicate if changes were made. The images or other third party material in this article are included in the article's Creative Commons licence, unless indicated otherwise in a credit line to the material. If material is not included in the article's Creative Commons licence and your intended use is not permitted by statutory regulation or exceeds the permitted use, you will need to obtain permission directly from the copyright holder. To view a copy of this licence, visit <http://creativecommons.org/licenses/by/4.0/>.

© The Author(s) 2024